Journal of Physics: Conference Series

PAPER • **OPEN ACCESS**

Model of thermal radiation using heat absorption by CO2 in submicron pores with application to magnesium-zinc ferrite fine disperse particles synthesis via combustion

To cite this article: A A Markov and I A Filimonov 2018 *J. Phys.: Conf. Ser.* **1009** 012040

Model of thermal radiation using heat absorption by CO2 in submicron pores with application to magnesium-zinc ferrite fine disperse particles synthesis via combustion

A A Markov[1] and I A Filimonov[2]

[1]Ishlinsky Institute for Problems in Mechanics RAS, Moscow 119526, Russia
[2]ISMAN RAS Chernogolovka, Moscow Region, 142432 Russia

E-mail: markov.ipm@yandex.ru

Abstract. Microscopic and macroscopic heat fluxes have been calculated on the basis of the self-consistent analysis of micro and macro scales taking into account absorption of thermal radiation by the CO2 molecules in micro pores. The macroscopic fluxes have been considered with the help of A. Shack modification to the Stefan-Boltzmann law at the given degree of blackness of a surface of a solid phase. These fluxes are received by averaging of the microscopic fluxes taking into account the influence of Knudsen's layer and absorption of heat during combustion of carbon. In the case of a submicron scale the models of slipping of a gas phase and jump of temperature of gas inside Knudsen's layers in the vicinity of pore borders are used. The intensities of macroscopic fluxes are presented through the parameters of similarity and depend on the emissivity of pore surfaces, on the coefficients of molecule reflection and thermal accommodation. The governing system of equations on a macroscopic scale includes heat exchange between the gaseous and solid phases. The macro fluxes are calculated by means of averaging of micro fluxes taking into account the effect of Knudsen's layer and the heat absorption during the carbon combustion. The synthesis of magnesium-zinc ferrite submicron particles is modelled numerically. The results of thermal front numerical simulation allow us to evaluate the impact of CO2 absorption, emissivity along with the slippage on the heat and mass transfer. It was found that an increase in the intensity of radiation corresponds to the decrease in the rate of submicron particles growth.

1. Introduction

At submicron scales when the size of a particle or of a pore filled with gas is less than the wavelength of radiation, the properties of absorption and emission significantly depend on the surface molecular structure.

Results and references concerning thermal radiation at submicron scales are presented in [1-6]. Measurements of thermal radiation in a nanometric gap between two golden plates [1, 2] have detected a heat flux which greatly exceeds the radiation limit of the absolutely black body. The obtained result was originally explained by the coupling of surface phonon modes inside the film, which creates additional channels for the photon tunneling [6].

The absorption and emission properties of clusters as systems of bound atoms are demonstrated to be the sources of thermal radiation that like the soot radiation in flames. The cluster properties are

reviewed in [4]. Peculiarities of absorption of thermal radiation by gas molecules are formulated in [7]. The approximate formulas for the heat absorption by molecules CO2 and H2O suggested by Schack with the Hottel's and Edgbert's modification are in good agreement with experimental data. The formulas are based on black-body radiation with given emissivity for gas and solid surface.

The mathematical models of self-propagating high temperature synthesis (SHS) of oxides or Combustion Synthesis (international name) are considered in numerous papers: [8-30]. The economical and energy efficient synthesis of nanostructured complex oxides from inexpensive reactant mixtures, referred to as Carbon Combustion Synthesis of Oxides (CCSO) was recently developed [8-11]. The CCSO is a modified form of the Self-propagating High-temperature Synthesis (SHS) or of so called internationally: Combustion Synthesis [16-18]. The experimental and numerical studies of CCSO have revealed that the gas transport behavior is rather complex with respect to traditional SHS systems. It involves at least two gaseous components: oxygen (oxygenator) as the main and practically unique gaseous reagent in SHS for gas-solid reactions and carbon dioxide which is released in the post combustion zone during CCSO. No carbon was used previously in original SHS systems [16]. Correspondingly, formation and release of carbon dioxide (the 2nd gas phase in CCSO) was not considered in models [18-20]. They were simpler in comparison with the multiphase gas dynamics taking place in CCSO [8-14, 26-30].

The effects of complex CCSO kinetics on dispersion of the CCSO condensed product are reported in [12-15, 24-30]. The models take into account in detail the gas dynamics as well as the mass and thermal transport accompanying CCSO. The result of theoretical predictions is in good agreement with experiments [28-30]. In SHS of materials, the thermal radiation is one of the fundamental mechanism of heat transfer. The characteristics of thermal radiation depends on various properties of the surface, including its temperature, its spectral absorptivity and spectral emissivity power, as is expressed by Kirchhoff's law. The simple approximation for the emitted power of radiation from particle surface into micro pore can be found using the Stefan-Boltzmann law for a gray body with a given emissivity [13, 31-33].

The estimates of radiation in combustion systems are given in [12, 21, 31-35]. The radiation can be neglected if the combustion temperature T_b doesn't exceed the critical value $T_b < T_{crit}^{rad}$. In the case of slow propagating front of carbon combustion synthesis of oxides (CCSO) [31-33] by smoldering combustion, the value of was estimated to be: $T_b << T_{crit}^{rad}$. Thus for slow CCSO the radiation impact is not important. The impact of radiation into the integral heat flux of slow CCSO [11] was estimated to be less than $6 \div 14\%$ while for fast CCSO for which the velocity of propagating combustion front $v_c \cong 4 mm/s$ the impact of thermal radiation rises up to $\cong 43\%$ and radiation should be taken into account.

During synthesis of submicron particles via CCSO the formation of Knudsen layer in gas close to pore surface becomes important [13, 14]. The models of slipping of a gas phase and jump of temperature of gas inside Knudsen's layers in the vicinity of pore borders are used.

The aim of the present research is to analyze the thermal radiation taking into account the CO2 absorption in submicron pores. The Shack's formula with the Hottel's and Edgbert's modification is applied [7]. According to [1, 2] the black-body model can be applied for length scales that are about 0.5 micron and more. For these scales the measured heat fluxes are not significantly differed from those predicted by the black-body radiation law. These length scales are considered in the present paper.

The approach applied is the generalization of the slip-jump technique [14]. The various intensity of macro fluxes due to gas velocity slippage on the surface of nanopores with allowance for a thermal radiation impact are simulated numerically. The temperature jump depends on the thermal reflection coefficient and on the thermal diffusivity. The radiation intensity, velocity slippage and temperature jump fluxes are formulated using the appropriate similarity parameters. The synthesis of magnesium-zinc ferrite submicron particles is modeled numerically. The results of thermal front numerical

simulation allow us to evaluate the impact of CO2 absorption, emissivity along with the slippage on the heat and mass transfer.

2. Simplified radiation equations at micro scale for isolated pore

In contrast to solids, gases have usually just lines, series of lines or bands as the spectra of absorption and radiation, i.e., the appreciable infrared (IR) absorption or radiation takes place only in certain local parts localized ranges of wavelength in of their spectrum (in so called absorption-emission bands), while solids have a continuous absorption-emission spectrum, since they absorb rays of any wavelength. Monatomic and diatomic gases practically do not absorb IR radiation. They are almost transparent in relation to IR radiation since a greater flux of energy (for example the high energetic UV radiation as in the case of nitrogen or oxygen) is needed for their excitement For a simplified calculation of radiation, a gray body model is used in which the area under the radiation intensity distribution curve via the wavelength is equal to the sum of the areas of the emission bands of the real gas. Because of the combustion acceleration due to gas slippage in submicron pores in the synthesis of particles behind the combustion front of carbon, it is necessary to take into account the IR absorption-emission of CO2. The emissivity of CO2 depends on the thickness of the gas layer and is proportional to the temperature $T^{3.5}$ while the flux density of the IR radiation from the solid phase is proportional to the temperature T^4.

The CO2 emission density per unit area of pore surface using Schack's formula [7] reads $E_{CO2} = 3.5 \times \sqrt[3]{l \cdot p_{CO2}} \left(T_g/100\right)^{3.5} \left(W/m^2\right)$. Here p_{CO2} is the partial pressure (bar), l is the average thickness of the layer (m), and T_g is the gas temperature (K°). The thickness of the layer depends on the shape of the pores and is proportional to the ratio of the pore volume to its area. The intensity of radiation and absorption of the pore surface according to the Stefan-Boltzmann law is equal to $E_S = \varepsilon_S c_0 \left(T_g/100\right)^4 \left(W/m^2\right)$, where $c_0 = 5.67$ is the Stefan-Boltzman constant, ε_S is the emissivity of the pore surface, T_g and T_S is the temperature of gas and solid phase.

Shack's formula with the Hottel's and Edgbert's modification, including the emissivity of the pore surface [7] is as follows
$q_{CO2} = 0.01 \cdot \varepsilon_S \cdot \left(p_{CO2} \cdot l\right)^{0.4} \left[\left(T_g/100\right)^{3.2} - \left(T_S/100\right)^{3.2} \times \left(T_g/T_S\right)^{0.65}\right] \left(W/m^2\right)$, where p_{CO2} – the partial CO2 pressure and l – the layer thickness.

2.1. Micro flow caused by thermal radiation on isolated pore surface

Our computations of slipping flow in an isolated tube showed the fast formation of steady state that depends only on radial (transverse) coordinate and doesn't depend on axial coordinate. The generalized Poiseuille flow using slippage boundary condition on the pore surface was obtained.
We begin with dimensional variables using cylindrical coordinates. Neglecting the advection transport, the steady state energy conservation equation reads

$$-\frac{1}{\mathrm{r}}\frac{\partial}{\partial \mathrm{r}}\left(\lambda_g\, r \frac{\partial T}{\partial \mathrm{r}}\right) = Q_{rad}^{micro}, \quad 0 < r < r_1 \tag{1}$$

Here Q_{rad}^{micro} denotes the micro heat flux due to thermal radiation. The equation (1) is solved using the symmetry and radiation boundary condition on the wall of a given pore

$$T^{/}\left(0\right) = 0 \text{ and } -\lambda_g T^{/}\left(r_1\right) = q_{CO2}$$

$$q_{CO2} = c_{02} \cdot \varepsilon_S \cdot \left(p_{CO2} \cdot r_1 \right)^{0.4} \left[-\left(\frac{T(r_1)}{100} \right)^{3.2} + \left(\frac{T_W}{100} \right)^{3.2} \times \left(\frac{T(r_1)}{T_w} \right)^{0.65} \right] \left(\frac{W}{m^2} \right)$$

and $c_{02} = 10.427 \ \left(WBa^{-0.4} m^{-2.4} K^{-3.2} \right)$. For the region close to the tube surface, we obtain

$$Q_{rad}^{micro} = c_{02} \times r_1^{-1} \cdot \varepsilon_S \cdot \left(p_{CO2} \cdot r_1 \right)^{0.4} \left[-\left(\frac{T(r_1)}{100} \right)^{3.2} + \left(\frac{T_W}{100} \right)^{3.2} \times \left(\frac{T(r_1)}{T_W} \right)^{0.65} \right]$$

2.2. Average fluxes for computation at macro step

Using the averaging over all pores inside the elementary volume V, we find the average flux as

$$\sum_l \int_{V_l} c_{02} \varepsilon_S r_1^{-1} \left[-\left(\frac{T(r_1)}{100} \right)^{3.2} + \left(\frac{T_W}{100} \right)^{3.2} \times \left(\frac{T(r_1)}{T_W} \right)^{0.65} \right]_l dV = V_{pore}^{\Sigma} c_{02} \varepsilon_S \hat{r}_1^{-1} \left[-\left(\frac{\hat{T}_g}{100} \right)^{3.2} + \left(\frac{\hat{T}_S}{100} \right)^{3.2} \times \left(\frac{\hat{T}_g}{\hat{T}_S} \right)^{0.65} \right]$$

The summation is assumed over all pores inside the given volume. Bar refers to the averaged values. Thus, the averaged dimensional radiation flux is:

$$Q_{rad}^{\dim} = \frac{\chi}{\hat{r}_1} c_{02} \cdot \varepsilon_S \cdot \left(\hat{p}_{CO2} \cdot \hat{r}_1 \right)^{0.4} \left[-\left(\frac{\hat{T}_g}{100} \right)^{3.2} + \left(\frac{\hat{T}_S}{100} \right)^{3.2} \times \left(\frac{\hat{T}_g}{\hat{T}_S} \right)^{0.65} \right] \left(\frac{W}{m^3} \right).$$

3. Frank-Kamenetskii dimensionless variables

We apply the time and length scales for combustion proposed by Frank-Kamenetskii [38]. The reference time scale and length scales are as follows:

$$t_0 = k^{-1} \exp\left(E \big/ RT_0 \right) \text{ and } l_0 = \sqrt{\frac{\lambda_0 t_0}{c_V \rho_0}}.$$

We use below the transformed non-dimensional variables marked with tilde above the letters. For Cartesian coordinates the variables read

$$\begin{aligned} &\tilde{x}_k = x_k / l_0, \ \ \tilde{t} = t/t_0, \tilde{u}_k = u_k / u_0, k = 1,2,3, \ u_0 = l_0 / t_0 \\ &\tilde{\rho}_{jg} = \bar{\rho}_{jg} / \rho_0 \ , j = 1,2, \ \tilde{\rho}_S = \bar{\rho}_S / \rho_0 \end{aligned} \tag{2}$$

Here $p_0 = R\rho_0 T_0 / M_0$ is the reference gas pressure. The effective density of gas and solid is marked with above bar (the mass of a given specie per unit volume occupied by this specie). $\bar{\rho}_g = \sum_j \bar{\rho}_{jg}$, $\rho_S = (1-\chi)\bar{\rho}_S$, $\rho_{jg} = \chi \bar{\rho}_{jg}$ where χ is a porosity. Using the similarity parameters $\beta = RT/E$, $\gamma = c_P T_0 \beta / Q$ the non-dimensional temperature is expressed as $\tilde{T} = (T - T_0) E \big/ \left(RT_0^2 \right)$; $T/T_0 = 1 + \beta \tilde{T}$. The dimensionless average macro heat flux due to thermal radiation can be presented in the form

$$\tilde{Q}_{g,rad}^{macro} = \frac{t_0 Q_{g,rad}^{\dim}}{\rho_0 c_g T_0} \text{ and } \tilde{Q}_{g,rad}^{macro} = \frac{A_R^0}{\beta} \tilde{p}_{CO2}^{0.4} \left(\frac{\left(1 + \beta \tilde{T}_G\right)^{0.65}}{\left(1 + \beta \tilde{T}_S\right)^{0.65}} \left(1 + \beta \tilde{T}_S\right)^{3.2} - \left(1 + \beta \tilde{T}_g\right)^{3.2} \right)$$

where the dimensionless intensity of thermal radiation is

$$A_R^0 = \chi \frac{c_{02}}{l_0 r_1} p_0^{0.4} \left(l_0 r_{pore}\right)^{0.4} \left(\frac{T_0}{10^2}\right)^{3.2} \times \frac{t_0}{\rho_0 c_g T_0}$$

and r_{pore} is dimensionless pore radius. For submicron pores, we take into account the formulas for the intensity of fluxes due to temperature jump and gas velocity slippage [14]. Thus, the heat flux due to temperature jump on the pores boundary reads

$$Q_{jump}^{macro} = \frac{2\chi}{r_1} \frac{\lambda_g \sqrt{\bar{\rho}_g P_g}}{\mu_g} \left(\frac{T_g}{T_W}\right)^{\alpha} \left(b_T \left(T_g - T_S\right) + b_W T_S\right) \left(\frac{W}{m^3}\right),\ b_T = \frac{\alpha'}{2-\alpha'} \sqrt{\frac{2}{\pi}} \frac{\gamma'+1}{2\gamma'},\ \gamma' = c_p / c_V$$

b_W characterizes the rate of a lateral pore surface cooling ($0 \le b_W \le 1$) and α' is the coefficient of thermal accommodation [14]. For the non-dimensional variables (2), we write down the macro heat flux due to temperature jump in the form

$$\tilde{Q}_{jump}^{macro} = A_T \sqrt{\tilde{\rho}_g \tilde{P}_g} \left(\left(-\tilde{T}_g + \tilde{T}_S\right) + \frac{b_W}{b_T \beta}\left(1 + \beta \tilde{T}_S\right)\right) \left(\frac{1+\beta \tilde{T}_g}{1+\beta \tilde{T}_S}\right)^{\alpha},\ A_T = \frac{2\chi b_T}{r_{pore}} \frac{l_0^2 \sqrt{\rho_0 P_0}}{\mu_0}$$

where A_T is the dimensionless temperature jump intensity.

The velocity slippage flux is given as $\vec{J}_{slip}^{macro} = 2\chi / \hat{r}_1\ b_u \sqrt{\bar{\rho}_g P_g}\,\mathbf{u}$ and $b_u = \theta\sqrt{2} \Big/ \left((2-\theta)\sqrt{\pi}\right)$, where θ is the reflection coefficient of gas molecules from the pores boundary, $0 \le \theta \le 1$. Applying the variables (2), we obtain $\tilde{J}_{slip}^{macro} = A_u \tilde{\mathbf{u}} \sqrt{\tilde{\rho}_g \tilde{P}_g}$. Here A_u is the dimensionless intensity of slippage

$$A_u = \frac{2\chi b_u}{r_{pore}} \frac{t_0 \sqrt{\rho_0 P_0}}{\rho_0} \quad \text{or} \quad A_u = \frac{2\chi b_u}{r_{pore}} \frac{l_0^2 \sqrt{\rho_0 P_0}}{\mathrm{Re}_0\, \mu_0}.$$

Using the local Mach and Reynolds numbers $Ma_0 = u_0 \sqrt{\rho_0} \Big/ \sqrt{\gamma P_0}$ and $\mathrm{Re}_0 = l_0 u_0 \rho_0 / \mu_0$ the intensities of fluxes can be expressed as follows

$$A_u = \frac{2\chi b_u l_0}{r_{pore}\sqrt{\gamma}} \frac{1}{Ma_0} \quad \text{and} \quad A_T = \frac{2\chi l_0 b_T}{r_{pore}\sqrt{\gamma}} \frac{\mathrm{Re}_0}{Ma_0 Pe_0}.$$

Estimates

The radiation intensity is evaluated as $A_R^0 = c_{02} p_0^{0.4} \left(l_0 r_{pore}\right)^{-0.6} \left(T_0/100\right)^{3.2} t_0 \left(\rho_0 c_g T_0\right)^{-1}$, using $t_0 = l_0^2 \rho_0 c_v / \lambda_0$, it follows $A_R^0 = \chi c_{02} p_0^{0.4} \left(l_0 r_{pore}\right)^{-0.6} \left(T_0/100\right)^{3.2} l_0^2 \left(T_0 \lambda_0 \gamma\right)^{-1}$. For reference values $l_0 \approx 10^{-5}$, $T_0 \approx 10^3$, $\mu_0 = 5 \cdot 10^{-5}$ we estimate $A_R^0 \approx \chi \left(r_{pore}\right)^{-0.6} l_0^{1.4} c_R$, where $c_R = c_{02} p_0^{0.4} T_0^{2.2} 10^{-6.2} \lambda_0^{-1}$ and $c_R \approx 10^5$. For pores of submicron size [13] $A_u \approx 200\chi b_u$ and $A_T \approx 200\chi b_T$.

4. The governing equations

The magnesium -zinc ferrite synthesis using the carbon combustion (CCSO) is considered. The kinetics [11] is applied:

$$\begin{aligned} &0.25\mathrm{MnCO_3(s)} + 0.75\mathrm{ZnO(s)} + \mathrm{Fe_2O_3(s)} + \mathrm{C(s)} + \mathrm{O_2(g)} \rightarrow \\ &0.25\mathrm{CO_2(g)} + \mathrm{Mn_{0.25}Zn_{0.75}Fe_2O_4(s)} \end{aligned} \tag{3}$$

The densities of gas species O2 and CO2 are $\rho_{1g} = \rho_{O2}$ and $\rho_{2g} = \rho_{CO2}$. The densities of solid species C, MnCO3, ZnO, Fe2O3, and magnesium- zinc ferrite are as follows

$\rho_{1S} = \rho_C$, $\rho_{2S} = \rho_{MnCO3}$, $\rho_{3S} = \rho_{ZnO}$, $\rho_{4S} = \rho_{Fe2O3}$, and $\rho_{5S} = \rho_{Fer}$

We use below the dimensionless variables (2), tilde is omitted. The mass conservation equation for total gas density reads

$$\frac{\partial \chi\rho_g}{\partial t} + \nabla\cdot\left(\chi\rho_g\,\mathbf{u}\right) = \left(1-\chi\right)J_{S\to g}^{macro}, \text{ where mass flux } J_{S\to g}^{macro} = \rho_{1S}\rho_{1g}k_1\exp\left(\frac{T_g}{\beta T_g+1}\right)$$

The mass conservation equations for gas species are $C_2 = 1 - C_1$

$$\chi\rho_g\frac{\partial C_1}{\partial t} + \chi\rho_g\mathbf{u}\nabla\cdot\left(C_1\right) = \nabla\cdot\left(\frac{\chi}{Pe_1}\rho_g\nabla C_1\right) - \left(1+\frac{M_{1g}}{M_{1S}}\right)J_{S\to g}^{macro},\quad 1+\frac{M_{1g}}{M_{1S}} = \frac{M_{2g}}{M_{1S}}$$

The mass conservation equations for solid species are as follows

$$\frac{\partial\rho_{1S}}{\partial t} = -\frac{M_{1S}}{M_{4S}}J_{S\to S}^{macro},\quad \frac{\partial\rho_{2S}}{\partial t} = -0.25\frac{M_{2S}}{M_{4S}}J_{S\to S}^{macro},\quad \frac{\partial\rho_{3S}}{\partial t} = -0.75\frac{M_{3S}}{M_{4S}}J_{S\to S}^{macro},\quad \frac{\partial\rho_{4S}}{\partial t} = -J_{S\to S}^{macro}$$

$$\frac{\partial\rho_{5S}}{\partial t} = \frac{M_{5S}}{M_{4S}}J_{S\to S}^{macro},\quad J_{S\to S}^{macro} = \rho_{2S}\rho_{3S}\rho_{4S}k_2\exp\left(\frac{T_S}{\beta T_S+1}\right) \text{ and } \rho_S = \sum_j\rho_{jS}$$

The momentum conservation includes the distributed porous resistance and the flux caused by gas slippage on porous surface

$$\frac{\partial\chi\rho_g\,\mathbf{u}}{\partial t} = \mathbf{S_V} + \vec{J}_{slip}^{macro} - \mathrm{Ma}^{-2}\nabla p_g + \mathrm{Re}^{-1}\nabla\cdot\boldsymbol{\tau};\quad \boldsymbol{\tau} = \mu\left[\nabla\mathbf{u} + \left(\nabla\mathbf{u}\right)^T - \frac{2}{3}\left(\nabla\cdot\mathbf{u}\right)\mathbf{I}\right]$$

The porous resistance and slippage fluxes are as follows

$$\left(\mathbf{S_V}\right)_i = -u_i\kappa_i,\quad \kappa_i = \alpha_i\left|u\right| + \varsigma_i\ ,i = 1,2,3.$$

The thermal balance for gas phase reads

$$\chi\rho_g c_g\left(\frac{\partial T_g}{\partial t} + \mathbf{u}\cdot\nabla T_g\right) = \nabla\cdot\left(\frac{\lambda_g}{Pe}\nabla T_g\right) - \kappa\left(T_g - T_S\right) + Q_{g,rad}^{macro} + Q_g^{macro} + Q_{jump}^{macro} \text{ and } Q_g^{macro} = QJ_{S\to g}^{macro}$$

The thermal fluxes caused by temperature jump and thermal radiation are

$$\vec{J}_{slip}^{macro} = A_u\mathbf{u}\sqrt{p_g\rho_g},\ Q_{jump}^{macro} = A_T\sqrt{\rho_g p_g}\left(\left(T_g - T_S\right) + \frac{b_W}{b_T\beta}\left(1+\beta T_S\right)\right)\left(\frac{1+\beta T_g}{1+\beta T_S}\right)^{\alpha} \tag{4}$$

$$Q_{g,rad}^{macro} = \frac{A_R^0}{\beta}\left(p_{CO2}\right)^{0.4}\left(\frac{\left(1+\beta T_g\right)^{0.65}}{\left(1+\beta T_S\right)^{0.65}}\left(1+\beta T_S\right)^{3.2} - \left(1+\beta T_g\right)^{3.2}\right) \tag{5}$$

The heat balance equation for solid phase reads

$$\left(1\text{-}\chi\right)\sum_j\rho_{jS}c_{jS}\frac{\partial T_S}{\partial t} = \nabla\cdot\left(\frac{\lambda_S}{Pe_T}\nabla T_S\right) + \kappa\left(T_g - T_S\right) + Q_{gS}^{macro} - Q_{g,rad}^{macro}$$

$$Q_{gS}^{macro} = Q\rho_{1S}\rho_{1g}k_1\exp\left(\frac{T_S}{\beta T_S+1}\right)$$

The heat exchange between solid and gas phases is described using the Leveque formula [38] that depends on Peclet and Reynolds numbers as follows $\kappa = \kappa_0 \left(1 + \mathrm{Re}_0^{0.3} Pe_T^{0.3}\right)$. The pressure satisfies the perfect gas equation $P_g = \rho_g \left(1 + \beta T_g\right)$.

5. Results of modelling and discussions

We report the carbon combustion simulation in a sample with submicron pores. The effect of thermal radiation, temperature jump as well as the velocity slippage on the pore surface has been analyzed. The results of computation of combustion presented below refer to the values of parameters as follows. $\beta \approx 0.1, \gamma \approx 0.288, \chi = 0.05$, where $\beta = RT_0/E$ and $\gamma = c_P T_0 \beta / Q$. The dimensionless resistance of porosity is given as $\alpha_i = 0$ and $\varsigma_i = 50$. The Mach and Reynolds number are $Ma_0 = 0.2$ and $\mathrm{Re}_0 = 10^{-2}$ The intensities of slippage, jump (4) and radiation (5) are given using the values: $A_u = 10^3$, $A_T = 10^2$, $\alpha = 0$, and $A_R^0 = 0, 10, 30, 400$. The thermal heat in the ignition is given as $q_f(t) = \begin{cases} \mathrm{Q_f}, 0 < t < t_{init} \\ 0, t \geq t_{init} \end{cases}$, where $\mathrm{Q_f} = 1200$. The ignition time is $t_{init} = 0.25 \div 0.5$. The cylindrical sample was placed in vertical position. The ignition initiated from the bottom at $x = 0$. In the figures below $0 \leq r \leq 1, 0 \leq x \leq 5$. The results of submicron particles is presented for radiation intensities: $A_R^0 = 0$, $A_R^0 = 10$, $A_R^0 = 30$, $A_R^0 = 400$, emissivity $\varepsilon_s = 0.85$, slippage intensity $A_u = 100$, and temperature jump $A_T = 10$. The data in figures 4÷8 refers to variable emissivity (5), which depends on CO2 partial pressure.

The influence of the heat CO2 absorption is demonstrated in figure 1 via gas temperature versus time distribution for various positions on the symmetry axis $(0,0), (0,0.3), (0,1), (0,1.5), (0,2)$, and $(0,3)$ lines 1, 2, 3, 4, 5, and 6.

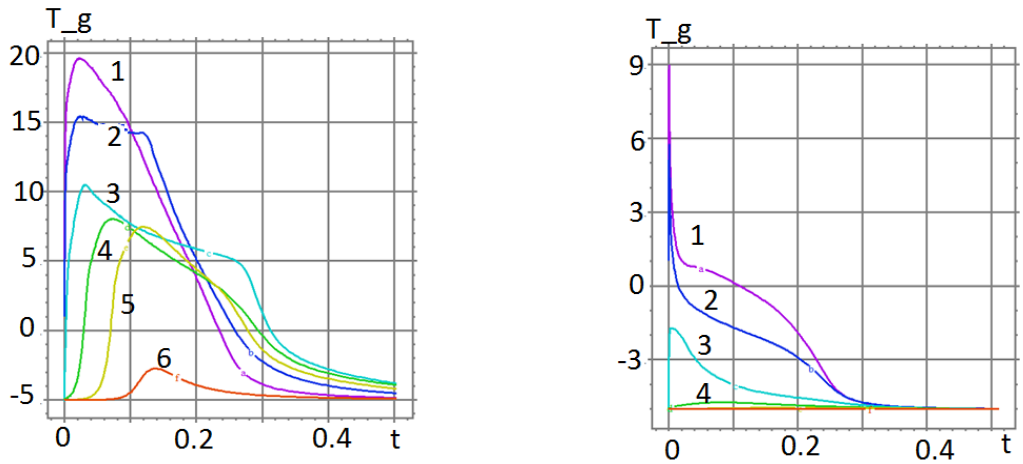

Figure 1. The CO2 heat absorption effect on the gas temperature is presented for radiation intensity $A_R^0 = 400$ -Temperature of the gas phase versus time on the axis of symmetry for positions with coordinates $(0,0), (0,0.3), (0,1), (0,1.5), (0,2)$, and $(0,3)$ lines $1 \div 6$ respectively is shown. Left and right column refers to the computation for constant emissivity of gas and variable one (5).

The radiation heat flux caused by CO2 molecules absorption results in remarkable (about double decrease) in the gas temperature (compare left and right columns in figure 1). The gas specie CO2 is generated just behind the combustion front. The heat absorbed in this region decreases both temperature and the velocity of the propagating combustion waves. Thus, neglecting the radiation

CO2 heat absorption gives the essential higher temperature maximum in combustion wave compared to the model that includes absorption (5).

Figure 2 shows the rate of propagating combustion front that is characterized by gas temperature versus time distribution for various positions $(0,0)$, $(0,0.3)$, $(0,1)$, $(0,1.5)$, $(0,2)$ and $(0,3)$ on the axis of symmetry of the sample. We can see the gas temperature decrease due to thermal radiation. The gas heat loss due to radiation absorption by CO2 molecules becomes higher with increasing values of radiation intensity. Using $A_R^0 \approx \chi\left(r_{pore}\right)^{-0.6} l_0^{1.4} c_R$ we conclude the remarkable lower gas temperature for smaller pore size.

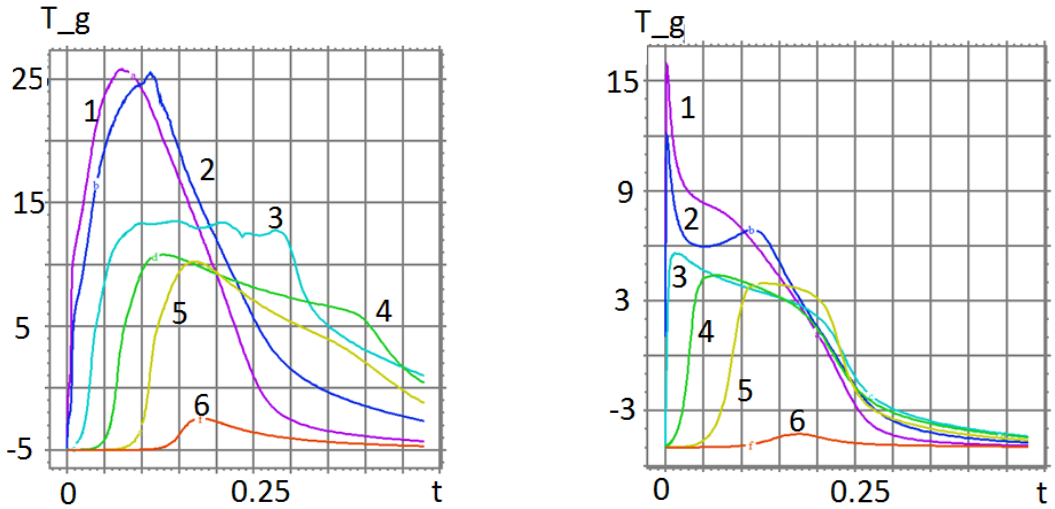

Figure 2. The temperature of gas phase versus time on the axis of symmetry for positions with coordinates $(0,0)$, $(0,0.3)$, $(0,1)$, $(0,1.5)$, $(0,2)$ and $(0,3)$ lines $1 \div 6$ respectively is shown. Left and right column refers to $A_R^0 = 0$ (no radiation) and to $A_R^0 = 10$ (variable emissivity (5)).

The solid temperature versus time on the symmetry axis is presented in figure 3. The radiation heat flux from gas to solid using (5) results in the increase of solid temperature. Radiation heat flux is provided by the sufficiently high temperatures of the solid.

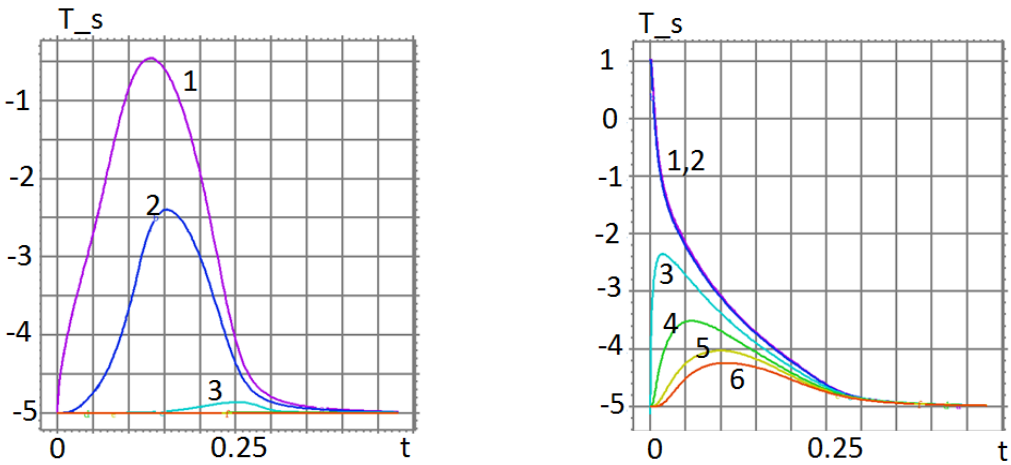

Figure 3. Temperature of solid phase versus time on the axis of symmetry for positions with coordinates $(0,0)$, $(0,0.3)$, $(0,1)$, $(0,1.5)$, $(0,2)$ and $(0,3)$ lines $1 \div 6$ respectively is shown. Left and right column refers to $A_R^0 = 0$ (no radiation) and to $A_R^0 = 10$ (the emissivity of gas depends on CO2 partial pressure).

The comparison of gas temperature for sufficiently big particle synthesis of $124\mu m$ and $1.7\mu m$ is shown in figure 4. Note the higher temperature and more intensive combustion takes place for bigger particles (see left column in figure 4).

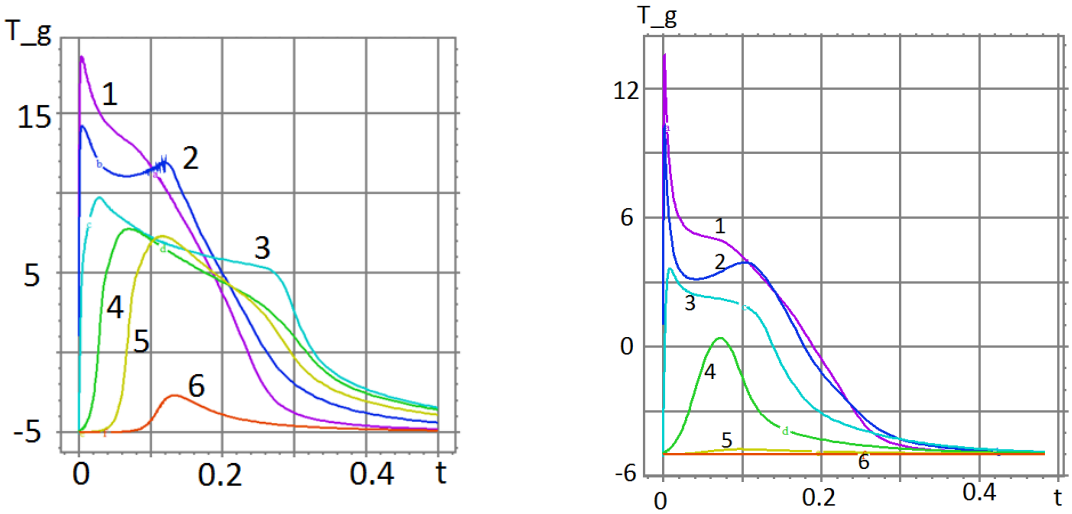

$A_R^0 = 2.3,\ r_{pore} = 124\mu m$ $A_R^0 = 30, r_{pore} = 1.7\mu m$

Figure 4. The temperature of gas phase versus time on the axis of symmetry for positions with coordinates $(0,0)$, $(0,0.3)$, $(0,1)$, $(0,1.5)$, $(0,2)$ and $(0,3)$ lines $1 \div 6$ respectively is shown. Left and right column refers to $A_R^0 = 2.3,\ r_{pore} = 124\mu m$ and $A_R^0 = 30, r_{pore} = 1.7\mu m$.

We estimated the radiation heat fluxes using the constant emissivity radiation for slipping model and the similar computation for which the emissivity of CO2 was varying with partial CO2 pressure (5). The comparison (see figure 1) demonstrates the remarkable increase of radiation heat fluxes for the constant emissivity computation. The rate of carbon oxide generation behind the propagating combustion front is illustrated in figure 5.

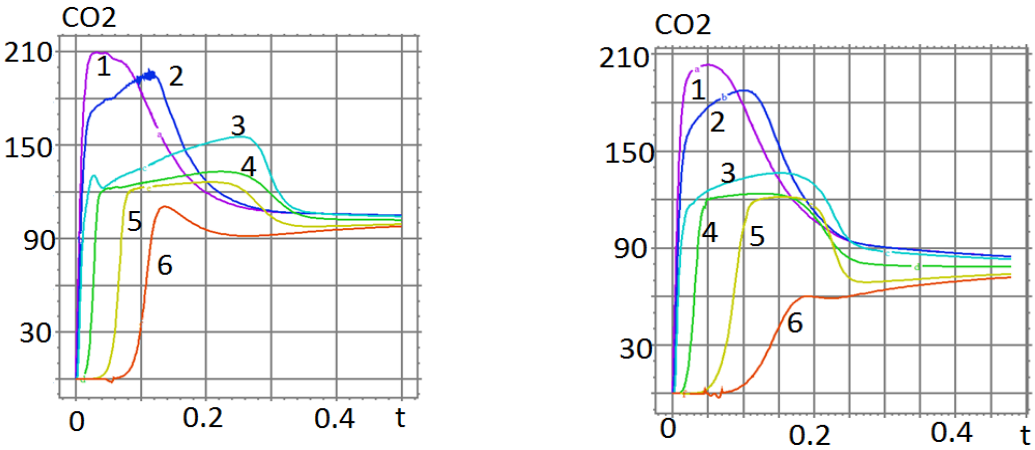

$A_R^0 = 2.3,\ r_{pore} = 124\mu m$ $A_R^0 = 10,\ r_{pore} = 10\mu m$

Figure 5. The CO_2 density versus time on the axis of symmetry for positions with coordinates $(0,0)$, $(0,0.3)$, $(0,1)$, $(0,1.5)$, $(0,2)$ and $(0,3)$ lines $1 \div 6$ respectively is shown. Left and right column refers to $A_R^0 = 2.3,\ r_{pore} = 124\mu m$ and $A_R^0 = 10,\ r_{pore} = 10\mu m$.

The significant higher gas pressure due to thermal radiation is found in pores of bigger size, i.e. for smaller radiation intensity, compare $A_R^0 = 10,\ r_{pore} = 10\mu m$ and $A_R^0 = 400, r_{pore} = 2nm$ in figure 6.

The density of magnesium-zinc ferrite at the same time instance $t = 0.5$ is shown in figure 7 for various intensities of radiation heat flux $A_R^0 = 2.3, 10, 30$, and 400 (see columns A,B,C, and D respectively). The heat lost due to thermal radiation results in the submicron particles synthesis retardation. This rate of slowness of synthesis is illustrated as well in figure 8 via reagent MnCO3 density distribution at the same time instance.

Note the difference of synthesis magnesium-zinc ferrite and nickel-zinc ferrite via combustion [11]. The CCSO synthesis of the $Mn_{0.25}Zn_{0.75}Fe_2O_4$ and $Ni_{0.35}Zn_{0.65}Fe_2O_4$ ferrites follows the reactions

$$0.25MnCO_3(s) + 0.75ZnO(s) + Fe_2O_3(s) + \alpha\left(C(s) + O_2(g)\right)$$

$$\rightarrow \left(\alpha + 0.25\right)CO_2(g) + Mn_{0.25}Zn_{0.75}Fe_2O_4(s) \text{ and}$$

$$0.35NiO(s) + 0.65ZnO(s) + Fe_2O_3(s) + \alpha\left(C(s) + O_2(g)\right)$$

$$\rightarrow Ni_{0.35}Zn_{0.65}Fe_2O_4(s) + \left(\alpha\right)CO_2(g)$$

The main difference between reactions of magnesium-zinc and nickel-zinc ferrite formation is that at the same content of carbon in the green mixture (that contains (α) moles of carbon) the greater amount of gaseous carbon dioxide is formed during the synthesis of magnesium-zinc ferrite. As one can see from the kinetic equations the magnesium-zinc ferrite synthesis is more promising than the synthesis of nickel-zinc ferrite in terms of gaseous carbon oxide generation since it produces $1 + 0.25/\alpha$ moles of carbon oxide per each mole of solid carbon contained initially in the green charge. While during the synthesis of nickel-zinc ferrite just about one mole of only is released per each mole of the carbon contained initially in the green mixture

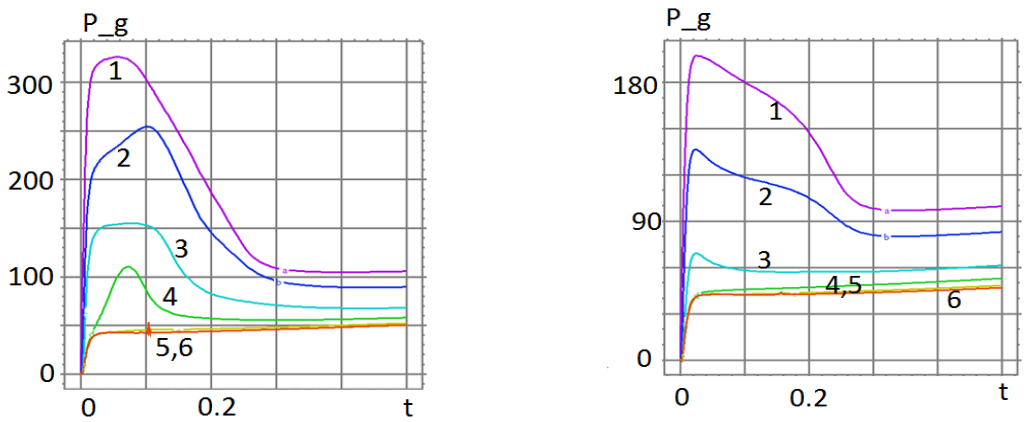

$A_R^0 = 10,\ r_{pore} = 10\mu m$ $A_R^0 = 400, r_{pore} = 2nm$

Figure 6. Pressure of gas phase versus time on the axis of symmetry for positions with coordinates $(0,0)$, $(0,0.3)$, $(0,1)$, $(0,1.5)$, $(0,2)$ and $(0,3)$ lines $1 \div 6$ respectively is shown. The emissivity of gas depends on CO2 partial pressure. Left and right column refers to radiation intensity $A_R^0 = 10$ and $A_R^0 = 400$.

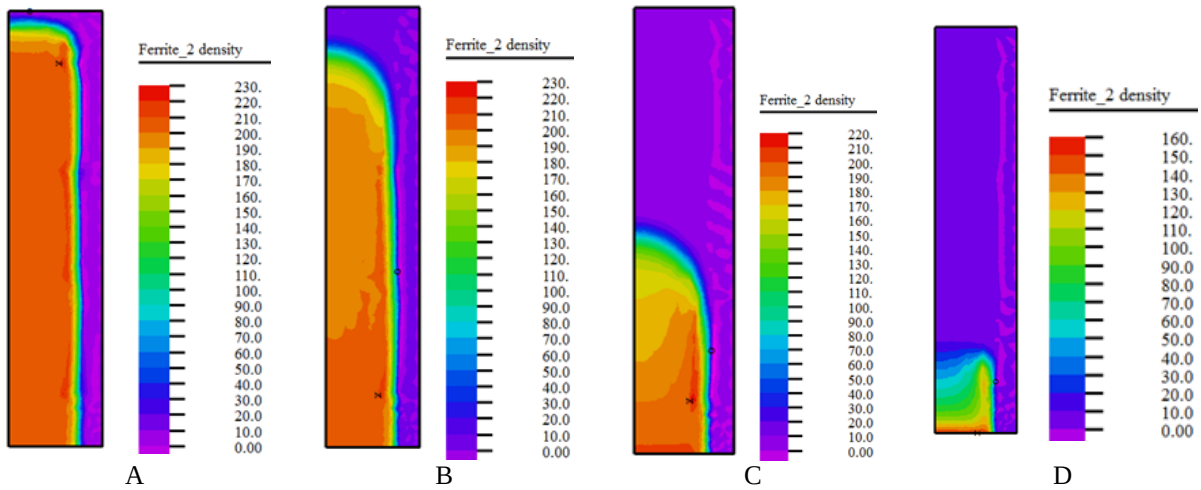

Figure 7. The product of synthesis $Mn_{0.25}Zn_{0.75}Fe_2O_4$ magnesium-zinc ferrite density in the reactor region $0<r<1;\ 0<z<5$ at the time instant $t=0.5$ is demonstrated. The columns A, B, C and D refer to increasing values of radiation intensity $A_R^0=2.3,\ 10,\ 30$ and 400 . The corresponding pore size is as follows $24\mu m,\ 10\mu m,\ 1.7\mu m$ and $2nm$.

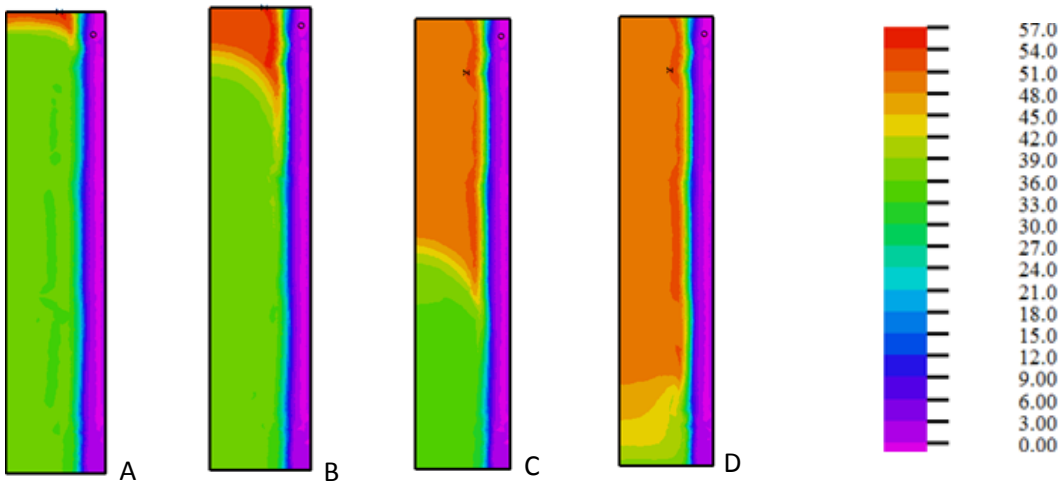

Figure 8. The reagent magnesium-zinc oxide $MnCO_3$ density when the emissivity of gas depends on CO2 partial pressure in the reactor region $0<r<1;\ 0<z<5$ at the time instant $t=0.5$ are shown for increasing values of radiation intensity $A_R^0=2.3,\ 10,\ 30$ and 400 . Column A, B, C, and D refers to $A_R^0=2.3,\ 10,\ 30$ and 400 respectively.

6. Conclusion

The fluxes induced by thermal radiation and velocity slipping fluxes in submicron pores as well as the fluxes of gas induced by temperature jumps are formulated using similarity parameters and applied in numerical simulation of the thermal front motion in a porous channel. The results allow us to predict characteristic features of the heat and mass transfer behind the thermal front in the sample with submicron pores. The significant impact of radiation as well as of velocity slipping for large Knudsen Number is reported. The results of thermal front numerical simulation allow us to evaluate and predict the impact of the CO2 emissivity and absorbtivity on the heat mass transfer including the effect of gas velocity slipping and temperature jump at submicron pore surface. An intense gas flow from the

combustion zone and the sample as a whole provides the excessive heat loss and decelerates propagation of the combustion wave during slipping.

We obtained that an increase in the intensity of radiation corresponds to the decrease of the submicron particles growth rate in CCSO wave.

The stronger slipping promotes the more intensive advection. The CO2 gas specie is generated intensively in the wave region close to a propagating combustion front from the side of products. The radiation heat flux caused by CO2 molecules absorption results in remarkable decreasing of the gas temperature and pressure. The smaller size of pores is considered the smaller value of gas temperature and pressure in pore is found.

List of principal notations

T'	Dimensional temperature
$T_0 = 1000^\circ C$	Referred temperature
$T = T'/T_0$	Dimensionless temperature
$\tilde{T} = (T-1)/\beta$	Dimensionless normalized temperature
T_g , T_{jS}	Gas temperature and solid phase temperature
T_{init}	Ignition temperature
$T_{initial}$, $T_{initial} = -1/\gamma$	Initial temperature of the sample
c_{Pk}	Specific capacity at constant pressure
ρ_{lg} , $l = 1,2$	Densities of gas species
$\rho_g = \rho_{1g} + \rho_{2g}$	Density of gas mixture
$\bar{\rho}_g$, $\bar{\rho}_S$, $\rho_g = \chi\bar{\rho}_g$, $\rho_S = (1-\chi)\bar{\rho}_S$	Effective values of gas density ρ_g and solid density ρ_S
$\beta = RT_0/E$	Dimensionless parameter
$\gamma = c_P T_0 \beta / Q$	Dimensionless parameter (Zeldovich number)
A_R^0	Dimensionless radiation heat parameter
$E_S = \varepsilon_S c_0 (T_g/100)^4 \ (W/m^2)$	Radiative flux
$c_0 = 5.67$	Stefan-Boltzmann constant
ε_S, $(0 \le \varepsilon_S \le 1)$	emissivity
$Pe_l = u_0 l_0 / D_{l,0}, l = 1,2$	Peclet numbers
$Pe = u_0 l_0 / \lambda_0$	Thermal Peclet number
$u_0 = l_0 / t_0$	Referred velocity
$\mathrm{Re}_0 = u_0 l_0 \rho_0 / \mu_0$	Reynolds number
χ	Porosity coefficient
P_0	Referred pressure
μ_0	Referred gas viscosity
λ_0	Referred thermal conductivity
Ma_0	Mach number
Q_f	Thermal flux
Q	Combustion heat

List of principal notations

$Q_{g,rad}^{macro}, Q_{g}^{macro}, Q_{jump}^{macro}$	Heat fluxes due to radiation, chemical reaction, and temperature jump
b_u; $b_u = \theta\sqrt{2}\Big/\left(\left(2-\theta\right)\sqrt{\pi}\right)$	Slip parameter
θ, $(0 \le \theta \le 1)$	Reflection coefficient
A_T	
$b_T = \sqrt{2/\pi}\,\alpha^{'}\left(\gamma^{'}+1\right)\Big/\left(\left(2-\alpha^{'}\right)2\gamma^{'}\right)$, $\gamma^{'} = c_p/c_V$	Temperature jump parameters
$\alpha^{'}$, $(0 \le \alpha^{'} \le 1)$	Thermal accommodation coefficient
D_T	Thermal diffusivity coefficient
R	Universal gas constant
$t_0 = k^{-1}\exp\left(E\big/RT_0\right)$, $l_0 = \sqrt{\lambda_0 t_0/(c_V\rho_0)}$	Referred time and length scales for the Frank-Kamenetskii variables
t_{init}	Ignition time

References

[1] Sheng S, Mavrokefalos A, Sambegoro P and Gang Chen G 2012 *Appl. Phys Let*. **100** (23) http://dx.doi.org/10.1063/1.4723713
[2] Sheng S Narayanaswamy A and Chen G 2009 *Nano Lett.* **9** (8) pp 2909–13 DOI: 10.1021/nl901208v http://pubs.acs.org/doi/abs/10.1021/nl901208v
[3] Martinenko Y and Ognev L 2005 *J. Tech. Phys*. **V. 75** (11) pp 130–32
[4] Smirnov B 1997 *Physics-Uspekhi* **40** (11):1117. (In Russian)
[5] Xi Liu X and Zhang Zh 2015 *ACS Photonics* Publication Date (Web): 17 Aug
[6] Xianglei Liu and Zhuomin Zhang 2015 Near-field thermal radiation between metasurfaces *ACS Photonics* ACS Photonics **2** (9) pp 1320–26 DOI: 10.1021/acsphotonics.5b00298
[7] Schack Alfred 1965 *Industrial Heat Transfer Practical and theoretical with basic numerical examples.* Translated from the 6th German ed. by I. Gutman Publisher: Springer US; Copyright Holder: Springer Science+Business Media New York. eBook ISBN: 978−1−5041−2079−1
[8] Martirosyan K S and Luss D 2005 Carbon Combustion Synthesis of Oxides: Process Demonstration and Features *AIChE.* **51** (10) pp 2801–10
[9] Martirosyan K Iliev M and Luss D 2007 *Internat. J. SHS* **16** (1) pp 36–45
[10] Martirosyan K S and Luss D 2009 *Chem. Eng. Technol*. **32** (9) pp 1376–83
[11] Martirosyan K S and Luss D 2007 Carbon Combustion Synthesis of Ferrites: Synthesis and Characterization *Ind. Eng. Chem. Res*. **46** pp 1492–99
[12] Markov A, Filimonov I and Martirosyan K 2012 *J. Comput. Phys*. **231** (20) pp 6714–24
[13] Markov A A 2015 Heat and Mass transfer in submicron pores at the movement of thermal front in a channel *Institute for Problems in Mechanics RAS Moscow (Preprint №1108*) p 45 (in Russian).
[14] Markov A 2014 *Computers and Fluids* **99** pp 83–92
[15] Markov A 2010 Micro and Macro Scale Technique for Particle Growth Simulation *Computational Fluid Dynamics Review* 2010 Chapter 24 pp 583–600
[16] Markov A, Barinov V, Umarov L and Filimonov I 2016 (in Russian) *Proc. NPNJ'2016* 25−31 May Alushta pp 97-99 ISBN 978-5-4316-0300-6
[17] Filimonov I and Poletaev A 2016 *Current Opinion in Chemical Engineering* **11** pp 42–45
[18] Rogachev A and Mukasyan A 2012 Combustion for synthesis of materials: Introduction into Structural Macrokinetics *Physmatlit* 398 p (in Russian)
[19] Merzhanov A 1997 *Reports of RAS* **503** (7) pp 353–55

[20] Merzhanov A, Peregudov A and Gontkovskaya V 1997 *Reports of RAS* **360** pp 217–19
[21] Filimonov I 1998 Combust. Explos. and Shock Waves **343** pp 69–76
[22] Zeldovich Y and Frank-Kamenetskii D 1938 *J Phys. Chem*. **12** pp 93–99
[23] Zeldovich Y 1942 *J of Experiment. and Theoret. Phys.* **12 (**11/12) pp 498–524
[24] Markov A, Filimonov I and Martirosyan K 2011 in: Kuzmin A (Ed.) *Comput. Fluid Dyn*. (Springer London) pp 929–936
[25] Markov A 2009 *Computers & Fluids* **38** pp 1435–44
[26] Markov A, Filimonov I and Martirosyan K 2013 *Internat. J. of SHS* **22** (1) pp 11–17
[27] MarkovA A, Hobosyan M A and Martirosyan K S 2016 Slip-Jump Model for Carbon Combustion Synthesis of Complex Oxide Nanoparticles *Eurasian Chemico-Technological Journal* **18** pp 223–32
[28] Markov A A, Hobosyan M A and Martirosyan K S 2015 Simulation of heat and mass transfer in pores as applied to synthesis of magnesium–zinc and nickel–zinc ferrite nanoparticles *Nanomechanics Science and Technology: An International Journal* DOI: 10.1615 Nanomechanics Sci.Technol.Int.J. **v6**. (i3.40) pp 209–22
[29] Markov A A, Hobosyan M A and Martirosyan K S 2016 Ferrite Synthesis Simulation via Carbon Combustion using Slip Temperature and Concentration Gas Species Jump at Pore Surface. *Physical-Chemical Kinetics in Gas Dynamics* **V16** (1) (in Russian)
[30] Markov A, Filimonov I, Hobosyan M and Martirosyan K 2016 *Wschodnioeuropejskie Czasopismo Naukowe (East European Scientific J.)* **9**(13) pp 58–63 http://eesa-journal.com/ru/o-zhurnale
[31] Filimonov I and Luss D 2005 *AIChE J*. **51** pp 1521–31
[32] Filimonov I 1998 *27th Intern. Symp on Combust.* (Boulder) pp 2441–50
[33] Filimonov I, Kidin N and Mukasyan A 2000 *Proc. of the Combust. Inst.* **28** pp 1421-29
[34] Seplyarskii B 2017 Abstracts of Internat. Conf Internat. SHS-50 dated for 50-year anniversary of SHS Chernogolovka (november 20-21st) p 192
[35] Seplyarskii B G et al 2014 *Mendeleev Communic.* **4** pp 242–44
[36] Karnidakis G, Beskok A and Aluru N 2005 *Microflows and nanoflows* Springer Science+Business Media Inc. p 817
[37] Kogan M 1967 Dynamics of rarefied gas *Moscow Nauka* p 440 (in Russian)
[38] Frank-Kamenetskii D A 1969 *Diffusion and Heat Transfer in Chemical Kinetics* (Second Enlarged and Revised Edition Translation Editor: J.P. Appleton Plenum Press) p 491
[39] Williams F A 1985 *Combustion theory* Westview Press p 704
[40] Koutateladze S 1970 *Basics of the Theory of Heat Exchange* Nauka Siberian Branch Novosibirsk p 658